

## MINIATURIZED MICROSTRIP DUAL-BAND BANDSTOP FILTERS USING TRI-SECTION STEPPED-IMPEDANCE RESONATORS

**K.-S. Chin and C.-K. Lung**

Chang Gung University  
Taoyuan 333, Taiwan, R.O.C

**Abstract**—A novel circuit structure of dual-band bandstop filters is proposed in this paper. This structure comprises two shunt-connected tri-section stepped impedance resonators with a transmission line in between. Theoretical analysis and design procedures are described. The derived synthesis equations have two degrees of freedom which provide more design flexibility in filter synthesis. Notably, three advantages of the proposed filter structure lie in the fact of its increased nonuniform impedances, resulting in a compact size, wide range of realizable frequency ratio, and more realizable impedances. Three experimental dual-band bandstop filters with various frequency ratios were fabricated to demonstrate the feasibility of the new filter structure.

### 1. INTRODUCTION

The dual-band or multi-band RF/Microwave system has become quite popular in recent years because of the need for wireless mobile communications. In a microwave communication system, the bandstop filter is an important component typically adopted in both receivers and transmitters. Dual-band bandstop filters (DBBSFs) are commonly employed in high-power amplifiers and mixers to suppress the double-sideband spectrum to reduce circuit size and cost.

Numerous structures and methods have been proposed for realizing dual-band filters [1–13]. The dual-stopband response can be determined by applying a two-step frequency-variable transformation to the low-pass prototype [1]. Chen et al. [2] integrated two stacked loops into a module for dual-mode dual-band operation.

---

Corresponding author: K.-S. Chin (kschin@mail.cgu.edu.tw).

Kuo et al. utilized a rigorous approach for designing dual-band bandpass filters in parallel-coupled and vertical-stacked configurations with stepped-impedance resonators [3]. The composite right/left-handed metamaterial transmission lines were implemented to replace the microstrip lines of conventional bandstop filters, yielding dual stopbands [4]. Cross-coupled filters constructed with split-ring resonators can also obtain two resonant frequencies [5].

Traditionally, open-ended quarter-wavelength stubs are widely used in single-band bandstop filters. Because the impedance of  $\lambda/4$  resonators is uniform, they have an electrical length of  $90^\circ$  at only a single frequency, which is not sufficient for dual-band application. Recently, parallel-connected stubs (named dual-behavior resonators) were proposed as composite shunt resonators to support dual-band performance [6–8]. The two-section or tri-section stepped-impedance resonators [9–12] have non-uniform impedances which can support  $90^\circ$  simultaneously at two resonant frequencies, thus they are suitable for dual-band operation and size reduction. However, the design of more compact dual-band filters is an ongoing challenge.

This work proposes tri-section stepped-impedance resonators (TSSIRs) to realize more compact dual-band bandstop filters. Two degrees of freedom exist for determining the dimensions of TSSIRs because of the under-determined feature of synthesis equations. The optimal structure of TSSIRs should comprise a wide middle section and a narrow top section to ensure good dual band operation and compactness. The experimental results agree closely with the simulation results, and a 23.6% size reduction is achieved by comparison with the conventional structures.

## 2. SYNTHESIS METHOD

### 2.1. Synthesis Equations

Traditionally, open-ended quarter-wavelength stubs are adopted in designing single-band bandstop filters, as presented in Fig. 1(a), because of their simplicity and ease of synthesis. These quarter-wavelength lines have an electrical length of  $90^\circ$  at only a single frequency because their impedance is uniform. Fig. 1(c) shows the configuration of the proposed tri-section stepped-impedance resonator which consists of three characteristic impedances and electrical lengths of  $(Z_1, \theta_1)$ ,  $(Z_2, \theta_2)$ , and  $(Z_3, \theta_3)$ . Since its impedance is non-uniform, tri-section stepped-impedance resonators can resonate at two different frequencies and be used in dual-band bandstop filter design. Additionally, the complexity of the structure enables the TSSIR to

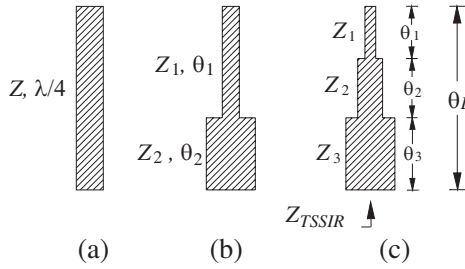


**Figure 1.** Configurations of (a) quarter-wavelength stub, (b) two-section stepped-impedance resonator, and (c) proposed tri-section stepped-impedance resonator.

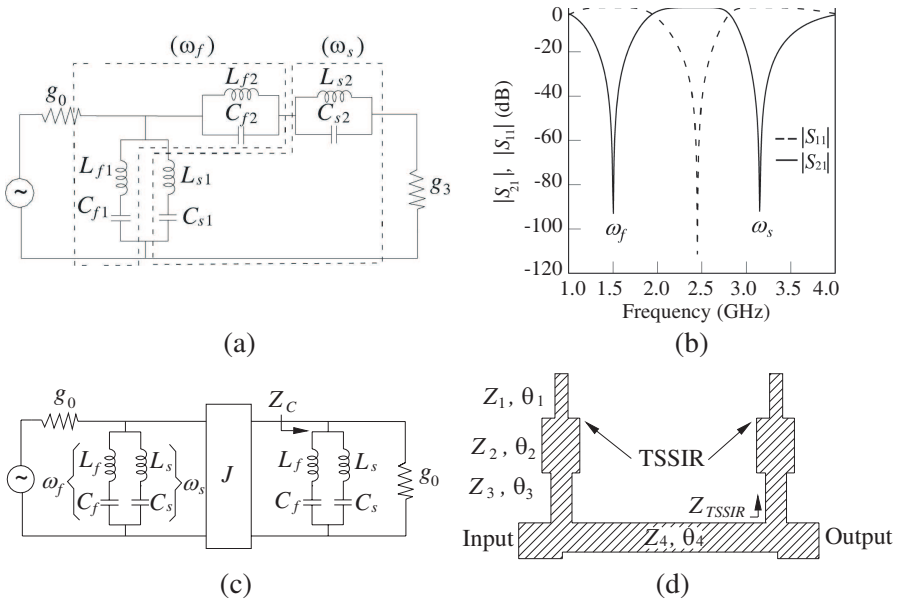


**Figure 2.** (a) Lumped-element circuit model of the second-order dual-band bandstop filter. (b) Simulated responses of Fig. 2(a). (c) Circuit model with all-shunt-connected series  $LC$  resonators and a  $J$  inverter. (d) Schematic of the proposed dual-band bandstop filter with TSSIRs.

be shorter than the two-section stepped-impedance resonator which is presented in Fig. 1(b).

Figure 2(a) shows the lumped-element circuit model of the proposed second-order dual-band bandstop filter. For performing two anti-resonance frequencies, the parallel and series association of two

bandstop structures are adopted. The dashed blocks indicate the two resonant circuits when the filter resonates at the first and second center frequencies  $\omega_f$  and  $\omega_s$ , respectively. When the series  $L_{f1}C_{f1}$  and parallel  $L_{f2}C_{f2}$  resonators resonate at  $\omega_f$ , the input signal is shorted and opened, respectively, to form a stop band. While the series  $L_{s1}C_{s1}$  and parallel  $L_{s2}C_{s2}$  resonators have very high and low impedances, respectively, they do not affect the input signal. A similar operation proceeds when the resonators of  $L_{s1}C_{s1}$  and  $L_{s2}C_{s2}$  resonate at  $\omega_s$ . Therefore, the circuit in Fig. 2(a) operates as a dual-band bandstop filter.

Designing with the frequencies of  $\omega_f$  and  $\omega_s$  and the associated bandwidths of  $\Delta_f$  and  $\Delta_s$ , the frequency mapping from the low-pass prototype to the bandstop yields the  $LC$  elements as  $L_{i1} = 1/\omega_i g_1 \Delta_i$ ,  $C_{i1} = g_1 \Delta_i / \omega_i$  (for series  $LC$ ) and  $L_{i2} = g_2 \Delta_i / \omega_i$ ,  $C_{i2} = 1/\omega_i g_2 \Delta_i$  (for parallel  $LC$ ), where  $g_i$  is the element value of the well-known low-pass filter prototype. As an example, Fig. 2(b) plots the simulated responses with dual frequencies of 1.5/3.15 GHz and bandwidths of 70/35%, where  $L_{f1} = 5.35$  nH,  $C_{f1} = 2.1$  pF,  $L_{f2} = 5.25$  nH,  $C_{f2} = 2.14$  pF,  $L_{s1} = 5.1$  nH,  $C_{s1} = 0.5$  pF,  $L_{s2} = 1.25$  nH, and  $C_{s2} = 2.04$  pF. It can be seen that two transmission zeros appear clearly at 1.5 and 3.15 GHz with more than 90 dB rejection level.

The series-connected parallel  $LC$  resonators can be transformed to all-shunt-connected series  $LC$  resonators with the aid of the admittance inverter  $J$ , as shown in Fig. 2(c). Fig. 2(d) shows the schematic of the proposed dual-band bandstop filter with TSSIRs.

As presented in Fig. 2(d), the input impedance of the tri-section stepped-impedance resonator  $Z_{TSSIR}$  can be derived as,

$$Z_{TSSIR} = jZ_3 \frac{\tan \theta_3 - Q(P \cot \theta_1 - Q \tan \theta_2)/(Q + P \cot \theta_1 \tan \theta_2)}{1 + Q \tan \theta_3 (P \cot \theta_1 - Q \tan \theta_2)/(Q + P \cot \theta_1 \tan \theta_2)}, \quad (1)$$

while the resonance condition  $Z_{TSSIR} = 0$  can be used to specify the two anti-resonance frequencies  $\omega_f$  and  $\omega_s$ . The impedance of the parallel-serial  $LC$  resonator  $Z_c$  in Fig. 2(c) is given by

$$Z_c = \frac{j}{\omega} \frac{\sqrt{L_f L_s} (\omega^2 - \omega_f^2) (\omega^2 - \omega_s^2)}{\omega_f \sqrt{C_f L_s} (\omega^2 - \omega_s^2) + \omega_s \sqrt{C_s L_f} (\omega^2 - \omega_f^2)} \quad (2)$$

which does not take into account  $g_0$ . The proposed TSSIR and its equivalent circuit should have the same reactance slope parameter,  $x = \omega_i/2 \cdot dX/d\omega|_{\omega_i}$  [15], to ensure the required bandwidths. Thus, the resonant condition  $Z_{TSSIR} = 0$  and the reactance slope parameter at the two resonant frequencies can be used to obtain four simultaneous

equations:

$$\tan \theta_3 = Q \frac{P \cot \theta_1 - Q \tan \theta_2}{Q + P \cot \theta_1 \tan \theta_2} \quad (3a)$$

$$\tan(r_f \theta_3) = Q \frac{P \cot(r_f \theta_1) - Q \tan(r_f \theta_2)}{Q + P \cot(r_f \theta_1) \tan(r_f \theta_2)} \quad (3b)$$

$$\frac{0.5Z_3 \sec^2 \theta_3 A}{[Q + P(\tan \theta_2 + Q \tan \theta_3) \cot \theta_1 - Q^2 \tan \theta_2 \tan \theta_3]^2} = \frac{1}{g_1 \Delta_f} \quad (3c)$$

$$\frac{0.5Z_3 r_f \sec^2(r_f \theta_3) B}{\{Q + P[\tan(r_f \theta_2) + Q \tan(r_f \theta_3)] \cot(r_f \theta_1) - Q^2 \tan(r_f \theta_2) \tan(r_f \theta_3)\}^2} = \frac{1}{g_1 \Delta_s} \quad (3d)$$

$$\begin{aligned} A = & P(Q^2 \theta_1 + QP\theta_2 + P\theta_3) \cot^2 \theta_1 \tan^2 \theta_2 + 2QP(1 - Q^2)\theta_3 \cot \theta_1 \tan \theta_2 \\ & + QP(Q\theta_1 + P\theta_2 + QP\theta_3) \cot^2 \theta_1 + Q^2(P\theta_1 + Q\theta_2 + Q^2\theta_3) \tan^2 \theta_2 \\ & + Q^2(P\theta_1 + Q\theta_2 + \theta_3) \end{aligned} \quad (3e)$$

$$\begin{aligned} B = & P(Q^2 \theta_1 + QP\theta_2 + P\theta_3) \cot^2(r_f \theta_1) \tan^2(r_f \theta_2) \\ & + 2QP(1 - Q^2)\theta_3 \cot(r_f \theta_1) \tan(r_f \theta_2) \\ & + QP(Q\theta_1 + P\theta_2 + QP\theta_3) \cot^2(r_f \theta_1) \\ & + Q^2(P\theta_1 + Q\theta_2 + Q^2\theta_3) \tan^2(r_f \theta_2) + Q^2(P\theta_1 + Q\theta_2 + \theta_3), \end{aligned} \quad (3f)$$

where  $r_f$  is the frequency ratio  $\omega_s/\omega_f$ , and  $\theta_1$ ,  $\theta_2$ , and  $\theta_3$  are all specified at the first resonant frequency  $\omega_f$ . Notably, only four synthesis equations are available for determining the six design parameters ( $\theta_1$ ,  $\theta_2$ ,  $\theta_3$ ,  $Z_1$ ,  $Z_2$ , and  $Z_3$ ) of the tri-section resonator, therefore,  $P$  and  $Q$  are chosen as the two degrees of freedom in finding the appropriate solutions. The six design parameters  $\theta_1$ ,  $\theta_2$ ,  $\theta_3$ ,  $P$ ,  $Q$ , and  $Z_3$  can then be determined by solving (3) simultaneously using a simple numerical analysis program.

## 2.2. Design Curves

A parametric study should be carried out to evaluate the design parameters of the tri-section stepped-impedance resonator as functions of  $P$  and  $Q$ . If the dual-band filter requires a second-order maximally flat response ( $g_1 = 1.4142$ ),  $r_f = 2.1$  (1.5 and 3.15 GHz),  $\Delta_f = 70\%$ , and  $\Delta_s = 35\%$ , then the impedance ratios  $P$  and  $Q$  can be initially set within the range 0.2–6.0 to find solutions. Here, the range of both  $P$

and  $Q$  is limited to 0.2–6.0 because the highest and lowest characteristic impedances of  $Z_1$ ,  $Z_2$ , and  $Z_3$  must be practical (typically, hi- $Z = 120\ \Omega$  and low- $Z = 20\ \Omega$ ).

Since the goal of the design is to minimize size, the best solution is obtained with  $P = 0.4$  to 2.4 and  $Q = 0.2$  to 0.7. Fig. 3 depicts the total electrical lengths  $\theta_L$  of the TSSIR that corresponds to various  $P$  and  $Q$ , where  $\theta_L = \theta_1 + \theta_2 + \theta_3$ . As presented in Fig. 3, all the values of  $\theta_L$  are below  $114^\circ$  when  $Q < 0.7$ . If the design includes a two-section stepped-impedance resonator, then the total length of the resonator would be  $116.15^\circ$  under the same criteria [9]. Therefore, the proposed TSSIR has a shorter length than the two-section stepped-impedance resonator. The  $\theta_L$  decreased as  $Q$  decreased, and all of the curves are U-shaped. Notably, the lowest point on the U-shaped

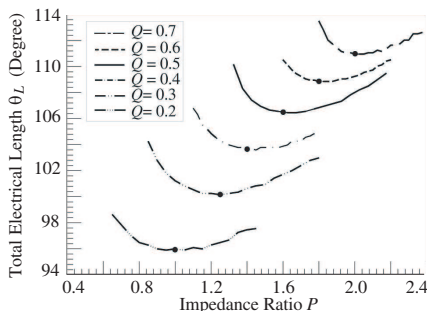


**Figure 3.** Computed total electrical length  $\theta_L$  versus impedance ratio  $P$  of TSSIR with various  $Q$  ( $r_f = 2.1$ ,  $\Delta_f = 70\%$ , and  $\Delta_s = 35\%$ ).

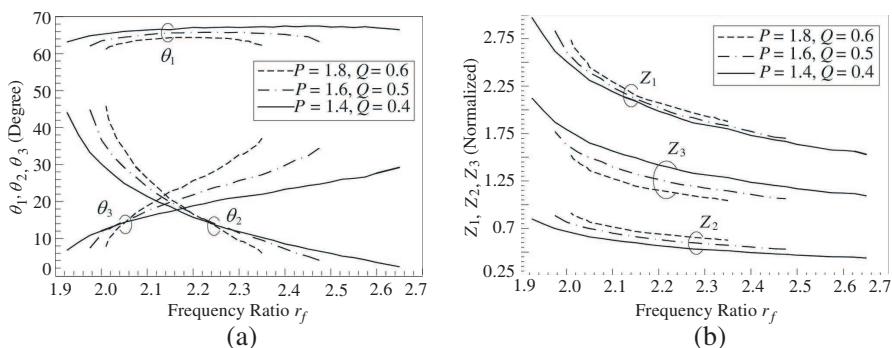


**Figure 4.** (a) Design curves of  $\theta_1$ ,  $\theta_2$ , and  $\theta_3$  with respect to  $r_f$ . (b) Normalized impedances  $Z_1$ ,  $Z_2$ , and  $Z_3$  versus  $r_f$  ( $\Delta_f = 70\%$ , and  $\Delta_s = 35\%$ ).

curve that corresponds to an optimal value of  $P$  which has the lowest  $\theta_L$ . Accordingly, each  $Q$  curve has a lowest  $\theta_L$  that corresponds to an optimum  $P$ . The lowest  $\theta_L$  can be reached at  $(P, Q) = (2, 0.7), (1.8, 0.6), (1.6, 0.5), (1.4, 0.4), (1.25, 0.3),$  and  $(1.0, 0.2)$ , as indicated by dots in Fig. 3.

Accordingly, when  $P > 1 > Q$ , which is when  $Z_1 > Z_3 > Z_2$ , the circuit size can be reduced efficiently. Since  $P > 1 > Q$  must be satisfied for reducing size, three cases in which  $(P, Q) = (1.8, 0.6), (1.6, 0.5),$  and  $(1.4, 0.4)$  are studied in Fig. 4 to show the design curves of the TSSIR versus frequency ratio  $r_f$  for filter synthesis. Fig. 4(a) plots the electrical lengths  $\theta_1, \theta_2,$  and  $\theta_3$  versus  $r_f$ .  $\theta_2$  monotonically decreases and  $\theta_3$  monotonically increases as  $r_f$  increases, while  $\theta_1$  remains almost constant. They satisfy  $\theta_1 > \theta_2 > \theta_3$  for  $r_f < 2.15$  and  $\theta_1 > \theta_3 > \theta_2$  for  $r_f > 2.15$ . When  $r_f$  is too high or low,  $\theta_2$  and  $\theta_3$  tend to be close to zero, and so the range of  $r_f$  is limited from 1.92 to 2.65, which still covers most of the design objectives. Detailed data show that the small pair  $(P, Q) = (1.4, 0.4)$  has the shortest total electrical length in the vicinity of  $r_f = 2.1$ . Notably, the parameters  $P$  and  $Q$  can not only be used to reduce size, but also can be used to change impractical impedances into more realizable ones.

Figure 4(b) plots the normalized impedances  $Z_1, Z_2,$  and  $Z_3$  as functions of  $r_f$ , where  $Z_1 = P \times Z_3$  and  $Z_2 = Q \times Z_3$  are the highest and lowest impedances of TSSIR, respectively. All of the impedances increase as  $r_f$  decreases. A larger pair  $(P, Q)$  is associated with higher impedance  $Z_1$ , which may cause difficulties because of the practical upper limit on impedance ( $120 \Omega$  typically). Thus, the total length must be traded off with line impedance to yield an appropriate combination of  $P$  and  $Q$ . If  $r_f = 2.1$  is required, then  $(P, Q) = (1.4, 0.4)$  would be a good choice both to shorten the length ( $\theta_L = 103.68^\circ$ ) and to realize impedances ( $Z_1 = 109.55 \Omega,$

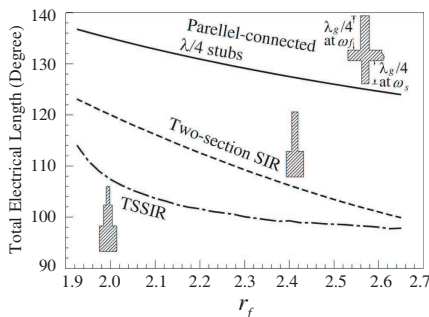


**Figure 5.** Total electrical length of proposed TSSIR versus  $r_f$  ( $\Delta_f = 70\%$ , and  $\Delta_s = 35\%$ ).

$Z_2 = 31.3 \Omega$ , and  $Z_3 = 78.25 \Omega$ ). Notably, as indicated in Fig. 4, various combinations of  $(P, Q)$  can also support a wide achievable range of  $r_f$ . Fig. 5 plots the total electrical length of the proposed TSSIR compared with the conventional parallel-connected  $\lambda/4$  stubs and the two-section stepped-impedance resonator. As shown in Fig. 5, the total length of TSSIR is less than in the other cases, and falls as  $r_f$  increases.

### 3. THREE EXAMPLES

The validity of the proposed tri-section stepped-impedance structure was examined experimentally by constructing three second-order maximally flat dual-band bandstop filters with various frequency ratios of 2.1 (1.5/3.15 GHz), 2.417 (2.4/5.8 GHz), and 2.85 (1.5/4.275 GHz). All filters were synthesized and fabricated on FR-4 DG (glass-epoxy double sided) substrates with  $\epsilon_r = 4.3$ ,  $\tan \delta = 0.02$ , and a thickness of 1.524 mm.

#### 3.1. Filter A (1.5/3.15 GHz, $r_f = 2.1$ )

The dual center frequencies of the first experimental filter were designed at 1.5 and 3.15 GHz with bandwidths of  $\Delta_f = 70\%$  and  $\Delta_s = 35\%$ , respectively. Solving (3) with  $g_1 = 1.4142$ ,  $r_f = 2.1$ ,  $P = 1.4$ , and  $Q = 0.4$  yields the designed parameters of TSSIR:  $Z_1 = 109.55 \Omega$ ,  $\theta_1 = 66.39^\circ$ ,  $Z_2 = 31.3 \Omega$ ,  $\theta_2 = 21.37^\circ$ ,  $Z_3 = 78.25 \Omega$ , and  $\theta_3 = 15.92^\circ$ . The design parameters of the simplified admittance inverter between TSSIRs can be calculated using  $\theta_4 = n\pi/(r_f + 1)$  and  $Z_4 = 1/|J \sin \theta_4|$  [9], yielding  $\theta_4 = 58.06^\circ$  and  $Z_4 = 58.92 \Omega$ . The calculated circuit dimensions and simulated responses of the experimental filter were then obtained using the full-wave EM simulator, IE3D. A network analyzer, HP 8510C, was employed for measurement, and the short-open-load-through (SOLT) technique was adopted for calibration.

Figure 6(a) compares the simulated and measured results for the first experimental filter: These results agree closely. The measured two mid-stopband frequencies were 1.495 and 3.11 GHz with corresponding bandwidths of 55% and 27%, respectively. If the conventional parallel-connected quarter-wavelength stubs and the two-section SIR are used with the same design specifications, then the required total electrical lengths are  $132.86^\circ$  and  $116.15^\circ$ , respectively. However, the electrical length of the proposed TSSIR is only  $103.68^\circ$ , and thereby achieves size reductions of 21.96% and 10.74% compared with the aforementioned parallel-connected  $\lambda/4$  stubs and two-section SIR, respectively. Fig. 6(b) displays a photograph of the fabricated filter A.

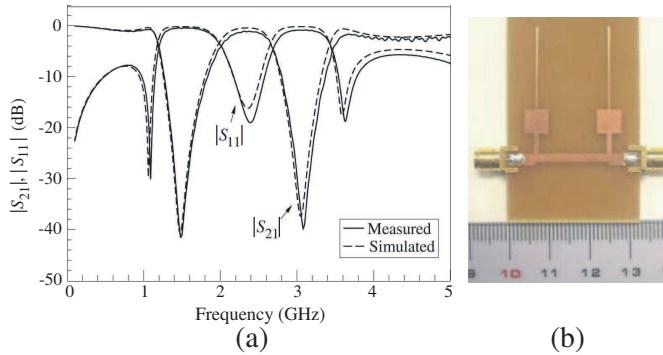


**Figure 6.** (a) Simulated and measured responses of filter *A*. (b) Photograph of filter *A*.

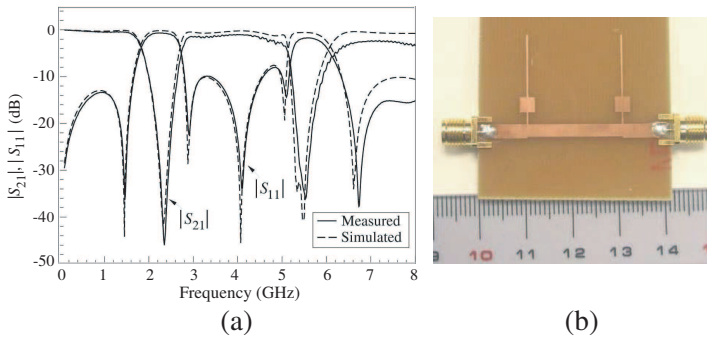


**Figure 7.** (a) Simulated and measured performances of filter *B*. (b) Photograph of filter *B*.  $Z_1 = 119.38 \Omega$ ,  $\theta_1 = 66.98^\circ$ ,  $Z_2 = 47.75 \Omega$ ,  $\theta_2 = 17.67^\circ$ ,  $Z_3 = 119.38 \Omega$ ,  $\theta_3 = 12.6^\circ$ ,  $Z_4 = 51.85 \Omega$ , and  $\theta_4 = 105.36^\circ$ .

**3.2. Filter *B* (2.4/5.8 GHz,  $r_f = 2.417$ )**

The two stop frequencies of filter *B* were designed at 2.4 GHz and 5.8 GHz bands ( $r_f = 2.417$ ) for a WLAN with bandwidths of 50% and 25%, respectively. Solving (3) with  $g_1 = 1.4142$ ,  $r_f = 2.417$ ,  $P = 1.0$ , and  $Q = 0.4$  yields the designed parameters of TSSIR as  $Z_1 = 119.38 \Omega$ ,  $\theta_1 = 66.98^\circ$ ,  $Z_2 = 47.75 \Omega$ ,  $\theta_2 = 17.67^\circ$ ,  $Z_3 = 119.38 \Omega$ ,  $\theta_3 = 12.6^\circ$ ,  $Z_4 = 51.85 \Omega$ , and  $\theta_4 = 105.36^\circ$ . Fig. 7(a) shows the comparison of the simulated and measured results of filter *B*, indicating that both responses have good agreement. The measured two mid-stopband frequencies were 2.35 and 5.58 GHz with corresponding bandwidths of 40.4% and 18%, respectively. If the conventional parallel-connected  $\lambda/4$  stubs are used for the same design specifications, the total electrical length requires  $127.24^\circ$ . Moreover, the electric length of the proposed

TSSIR is only  $97.25^\circ$ , which a size reduction 23.6% is achieved. Fig. 7(b) is the photograph of filter *B*.

### 3.3. Filter *C* (1.5/4.275 GHz, $r_f = 2.85$ )

The third filter *C* was designed at 1.5/4.275 GHz ( $r_f = 2.85$ ) with bandwidths of 50% and 25%, respectively. The circuit dimensions are  $Z_1 = 97.63 \Omega$ ,  $\theta_1 = 76.09^\circ$ ,  $Z_2 = 39.05 \Omega$ ,  $\theta_2 = 5.98^\circ$ ,  $Z_3 = 97.63 \Omega$ ,  $\theta_3 = 10.85^\circ$ ,  $Z_4 = 50.1 \Omega$ , and  $\theta_4 = 93.51^\circ$ . Fig. 8(a) shows the simulated and measured results of filter *C*. The measured two mid-stopband frequencies were 1.48 and 4.21 GHz with corresponding bandwidths of 41.22% and 17.82%, respectively. Fig. 8(b) is the photograph of filter *C*. Table 1 lists the performances of the three

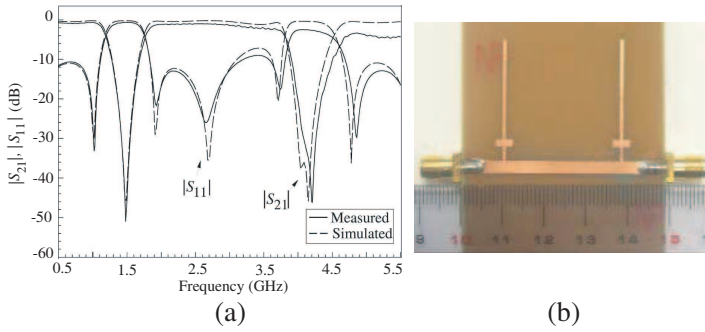


**Figure 8.** (a) Simulated and measured responses of filter *C*. (b) Photograph of filter *C*.

**Table 1.** Performances of the three experimental dual-band filters.

Filter		Center Frequency (GHz)	Bandwidth (%)	Rejection Level (dB)	Size Reduction (%)
A	Design	1.5/3.15	70/35	–	21.96
	Measured	1.495/3.11	55/27	39.8/42	
B	Design	2.4/5.8	50/25	–	23.57
	Measured	2.35/5.58	40.4/18	46/40	
C	Design	1.5/4.275	50/25	–	23.6
	Measured	1.48/4.21	41.22/17.82	50/46	

experimental dual-band filters, where the size reduction is compared with the conventional parallel-connected  $\lambda/4$  stubs.

#### 4. CONCLUSION

A novel circuit structure of dual-stopband filters is presented in this work. This compact dual-stopband filter has fully controllable center frequencies and bandwidths. The proposed tri-section stepped-impedance resonators allow designers to have more design flexibility in filter synthesis. Three advantages of the compact size, wide range of realizable frequency ratio, and more realizable characteristic impedances can be achieved by choosing a suitable pair  $(P, Q)$  in the synthesis formulas. The design procedures are discussed in detail, and the design curves are also provided. Three microstrip dual-band bandstop filters have been successfully designed with reduced sizes up to 23.6% by using the proposed resonators, and measured results match well with the simulated responses.

#### ACKNOWLEDGMENT

This work was partially supported by the National Science Council, Taiwan, R.O.C., (NSC 97-2221-E-182-015) and Chang Gung University, Taiwan, R.O.C., (UERPD280061). We also like to thank the support of High Speed Intelligent Communication (HSIC) Research Center, Chang Gung University.

#### REFERENCES

1. Uchida, H., H. Kamino, K. Totani, N. Yoneda, M. Miyazaki, Y. Konishi, S. Makino, J. Hirokawa, and M. Ando, "Dual-band-rejection filter for distortion reduction in RF transmitters," *IEEE Trans. Microwave Theory Tech.*, Vol. 52, 2550–2556, Nov. 2004.
2. Chen, J.-X., T. Y. Yum, J.-L. Li, and Q. Xue, "Dual-mode dual-band bandpass filter using stacked-loop structure," *IEEE Microw. Wireless Compon. Lett.*, Vol. 16, 502–504, Sep. 2006.
3. Kuo, J.-T., T.-H. Yeh, and C.-C. Yeh, "Design of microstrip bandpass filters with a dual-passband response," *IEEE Trans. Microwave Theory Tech.*, Vol. 53, 1331–1337, Apr. 2005.
4. Tseng, C.-H. and T. Itoh, "Dual-band bandpass and bandstop filters using composite right/left-handed metamaterial transmission lines," *IEEE MTT-S Int. Microwave Symp. Dig.*, 931–934, 2006.

5. Fan, J.-W., C.-H. Liang, and X.-W. Dai, "Design of cross-coupled dual-band filter with equal-length split-ring resonators," *Progress In Electromagnetics Research*, PIER 75, 285–293, 2007.
6. Quendo, C., E. Rius, and C. Person, "Narrow bandpass filters using dual-behavior resonators," *IEEE Trans. Microwave Theory Tech.*, Vol. 51, 734–743, Mar. 2003.
7. Tsai, C.-M., H.-M. Lee, and C.-C. Tsai, "Planar filter design with fully controllable second passband," *IEEE Trans. Microwave Theory Tech.*, Vol. 53, 3429–3439, Nov. 2005.
8. Ma, Z., K. Kikuchi, Y. Kobayashi, T. Anada, and G. Hagiwara, "Novel microstrip dual-band bandstop filter with controllable dual-stopband response," *Asia-Pacific Microwave Conference Proceedings*, 1177–1180, Dec. 2006.
9. Chin, K.-S., J.-H. Yeh, and S.-H. Chao, "Compact dual-band bandstop filters using stepped-impedance resonators," *IEEE Microw. Wireless Compon. Lett.*, Vol. 17, No. 12, 849–851, Dec. 2007.
10. Zhang, H. and K. J. Chen, "Miniaturized coplanar waveguide bandpass filters using multisection stepped-impedance resonators," *IEEE Trans. Microwave Theory Tech.*, Vol. 54, 1090–1095, Mar. 2006.
11. Yeh, L.-K., C.-Y. Hsu, C.-Y. Chen, and H.-R. Chuang, "A 24-/60-GHz CMOS on-chip dual-band bandpass filter using trisection dual-behavior resonators," *IEEE Electron. Device Lett.*, Vol. 29, No. 12, 1373–1375, Dec. 2008.
12. Chin, K.-S. and J.-H. Yeh, "Dual-wideband bandpass filter using short-circuited stepped-impedance resonators," *IEEE Microw. Wireless Compon. Lett.*, Vol. 19, No. 3, 155–157, Mar. 2009.
13. Wang, X.-H., B.-Z. Wang, and K. J. Chen, "Compact broadband dual-band bandpass filters using slotted ground structures," *Progress In Electromagnetics Research*, PIER 82, 151–166, 2008.
14. Pozar, D. M., *Microwave Engineering*, 3rd Edition, John Wiley & Sons, New York, 2005.
15. Matthaei, G. L., L. Young, and E. M. T. Johns, *Microwave Filters, Impedance Matching Networks, and Coupling Structures*, Artech House, Norwood MA, 1980.